Oxid Met (2013) 80:529–540
DOI 10.1007/s11085-013-9394-y

ORIGINAL PAPER

Fireside Corrosion of Superheater Materials in Coal/Biomass Co-fired Advanced Power Plants

Tanvir Hussain · Adnan U. Syed · Nigel J. Simms

Received: 25 May 2012 / Published online: 15 March 2013

Abstract A series of laboratory-based fireside corrosion exposures were conducted to assess the effect of such conditions on superheater/reheater materials at higher than conventional metal temperatures. Controlled atmosphere furnaces combined with the "deposit recoat" test method were used to generate the exposure conditions; the gaseous environment simulated that anticipated from air-firing 20 wt% cereal co-product mixed with a UK coal. The exposures were carried out at 600, 650 and 700 °C with four candidate materials: T92, HR3C and 347HFG steels; nickel-based alloy 625. After the exposures, the samples were examined by SEM/EDX to characterize the damage. Pre- and post-exposure dimensional metrology were used to quantify the metal damage in terms of metal loss distributions. For the austenitic steels, the combined deposit/gas/temperature exposure conditions enabled quantification of the characteristic 'bell-shaped' curves (of damage as a function of temperature) for fireside corrosion.

Keywords Fireside corrosion · Superheater corrosion · Coal/biomass co-firing · Air- firing

Introduction

CO_2 emissions from conventional fossil fuel fired power plants are believed to be a significant contributor to the enhanced greenhouse effect/global warming. There are

T. Hussain · A. U. Syed · N. J. Simms (✉)
Cranfield University, Cranfield, Bedfordhsire MK43 0AL, UK
e-mail: n.j.simms@cranfield.ac.uk

T. Hussain
e-mail: t.hussain@cranfield.ac.uk

A. U. Syed
e-mail: adnan.syed@cranfield.ac.uk

currently various legislations at national and EU levels for CO_2 emission reduction. Reduced CO_2 emissions from pulverized coal-fired power plants can be achieved by increasing the operating temperatures (and pressures) of their steam systems (which in turn increases the overall efficiency of the plants) and by using "carbon-neutral" fuels such as biomass.

Biomass is a major contributor to renewable energy production, accounting for approximately 70 % of worldwide renewable energy production [1]. Power plants burning biomass alone as fuel face significant issues with fouling, deposition, agglomeration and corrosion, which restrict the steam temperatures that can be used and so reduce the overall efficiency of the plants. However, these issues can be reduced by the co-firing of biomass and coal. The existing coal fired stations are both much larger and more efficient than new biomass plants, so a few percentage of biomass fed into an existing large coal power station will provide more biomass derived renewable energy than a new dedicated biomass station using the same amount of biomass. The introduction of biomass can be achieved by relatively minor modifications to the existing coal-fired plants and so avoids the large capital costs of building a new dedicated biomass plant.

Increasing the power generation efficiency by moving gradually towards higher steam operating temperatures (and pressures) has been underway for many years. However, increases in boiler component operating temperatures present many challenges for materials, including creep and fatigue, as well as fireside issues. Fireside corrosion has been a life limiting factor for the power generating industry where coal has been used as a fuel [2]. Fireside corrosion (i.e. metal loss of heat exchangers due to chemical reactions with the surrounding environment at high temperature) can lead to failure of boiler tubes (superheater, reheater, waterwalls) either by general metal loss or by the formation of cracks that then allows failure to occur by mechanical damage. In pulverized coal boilers alkali-iron tri-sulfates can form in the deposits on the superheaters/reheaters which have been identified by a number of researchers as the key factor in superheater metal loss [2, 3]. Fireside corrosion takes places when heat exchanger materials react with a combination of combustion gases (SOx, HCl) and surface deposits, ultimately resulting in tube failure. Such failures are very expensive to repair and result in unscheduled plant down time. Since the introduction of biomass, the issue of fireside corrosion has become more significant. In addition, the higher operating temperatures in future power plants will result in higher than acceptable metal losses for conventional superheater/reheater materials and may require the use of a new generation of materials (e.g. nickel based alloys). Unless preventative action is taken, the increased steam system operating temperatures combined with co-firing of coal with biomass will have a significant effect on the fireside corrosion of the heat exchanger materials.

This paper reports the results of an investigation into the fireside corrosion of superheater/reheater materials at metal temperatures higher than the average conventional temperatures of existing pulverized fuel power plants when air-firing of a specific biomass-UK coal fuel mixture. The fireside corrosion exposures were carried out at 600, 650 and 700 °C in simulated air-fired combustion gases on T92, 347HFG, HR3C and 625 alloys. The tests were carried out using the established

"deposit-recoat" technique that was developed for high temperature corrosion in various environments [4–6]. Dimensional metrology has been utilized as the primary tool to quantify the metal damage occurring in the specific corrosive environments.

Experimental Procedures

In this study, one ferritic steel (T92), two austenitic steels (347 HFG, HR3C) and one nickel-based alloy (625) were used to represent candidate materials for superheaters/reheaters in advanced pulverized fuel power plants. The nominal compositions of the alloys are presented in Table 1. The alloys were sourced as long boiler tubes which were then cut and machined into tube segments with dimensions of $\sim$15 mm chord, 15 mm long and 4 mm wall thickness. All the sample surfaces were prepared to a UK 600 grit surface finish.

The exposure conditions were set following a detailed study of the gaseous environments and deposit conditions that could be found around superheaters/reheaters in conventional air and pulverized fuel fired power stations, but using various biomass-coal fuel combinations [3, 7]. For these fireside corrosion exposures, the gaseous conditions were based on co-firing 80:20 wt% of a typical UK coal (Daw Mill) coal with CCP. The detailed composition of the coal and biomass fuels and the method of simplification to key active components had been described in detail in previous papers (e.g. [8]). The nominal compositions of the gas in air-firing condition are given in Table 2. The alloys were tested at 600, 650 and 700 °C both without any deposit (referred to as D0) and with a standard deposit (referred to as D1, with the composition given in Table 3). D1 is a widely used standard deposit for screening tests in fireside corrosion as it represents a composition of alkali-iron tri-sulfate that has been identified in many studies as being the principle cause of fireside corrosion on superheaters/reheaters in pulverized coal fired stations [2, 3, 9–11].

The fireside corrosion exposures were carried out in an alumina lined vertical controlled-atmosphere furnace using simulated air-fired combustion gases. A schematic diagram of the fireside corrosion tests is shown in Fig. 1. The furnace accommodates 24 test pieces in alumina crucibles at one time in the hot zone. Each test was run for 1,000 h using the widely accepted "deposit-recoat" method [4–6].

Table 1 Nominal composition of alloys used in fireside corrosion exposures (data in wt%)

Materials	Cr	Mo	Ni	Si	Mn	P	S	C	Fe	Others
T92	9.5	0.6		≤0.5	≤0.6	≤0.02	≤0.01	0.13	Bal.	0.25 V; 2 W; 0.09 Nb; 0.07 N
347 HFG	17–19		9–13	≤0.5	≤2	≤0.045	≤0.03	0.08	Bal.	0.6 < Nb + Ta < 1
HR3C	25		20	0.75	≤2	≤0.04	≤0.04	0.1	Bal.	0.4 Nb; 0.2 N
Alloy 625	20–23	8–10	Bal.	≤0.5	≤0.5	≤0.015	≤0.015	0.01	5	1 Co; 0.4 Al

Table 2 Nominal gas compositions used in fireside corrosion exposures

N_2 (vol%)	O_2 (vol%)	CO_2 (vol%)	H_2O (vol%)	SO_2 (vppm)	HCl (vppm)
Balance	4	14	8	1,300	400

Table 3 Deposit compositions used in fireside corrosion exposures (composition in mol%)

	Na_2SO_4	K_2SO_4	Fe_2O_3
D0 (bare)	–	–	–
D1	37.5	37.5	25

Prior to sample exposure, the samples were cleaned using a degreaser (volasil) followed by isopropanol (IPA) in an ultrasonic bath for 20 min. For those samples being exposed with a surface deposit, the cleaned samples were painted using a paint brush to apply a deposit loading of $\sim$20 mg/cm^2. The test was cycled every 200 h and repainted with deposits to replenish any salts, resulting in a deposition flux of 100 μg/cm^2 h. As part of the deposit-recoat process [5], the samples were weighed every 200 h both with and without crucibles as well as before and after applying the deposits.

Premixed gases were supplied to the controlled-atmosphere furnace through mass flow controllers to achieve the desired gas composition. The gas containing (CO_2, O_2, N_2) was passed through a de-ionized water bubbler which was kept at 40 °C in a water bath to add the required amount of moisture to the gas stream before mixing with the corrosive species (HCl, SO_2).

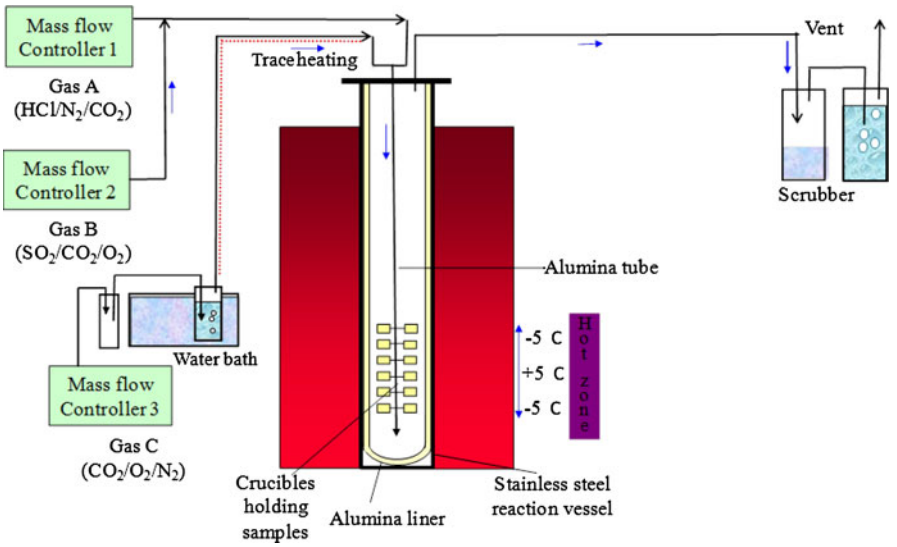

Fig. 1 Schematic diagram of a controlled atmosphere furnace setup for fireside corrosion in simulated air-firing combustion gases

The exposed samples were vacuum mounted using a low shrinkage cold mounting resin filled with ballotini (to further reduce shrinkage) in a specially designed jig and cross-sectioned, ground and polished to 1 μm diamond grit finish using non-aqueous lubricants. The polished cross-sections were examined in an Environmental Scanning Electron Microscope (ESEM) to investigate the scale layer thicknesses and microstructures. Energy dispersive X-ray (EDX) spectroscopy was used to identify the composition of the scales/deposits on the cross-sections. EDX mapping was also used to identify the elemental distribution of key components across the scale/metal interfaces.

The dimensional metrology of the samples before and after exposure is a key element of this work. All samples were measured using a digital micrometer (with resolution of 1 μm) prior to their exposure. Post-exposure of sample cross-sections was carried out, using an image analyzer connected to an optical microscope with a motorized x–y co-ordinate table, to determine the remaining metal thickness and any internal damage. The measured co-ordinates from the post-exposure image analysis were transferred into spreadsheets and compared with the pre-exposure micrometer measurements to determine metal loss data distributions for each sample. These distributions can be further processed, for example to generate cumulative probability curves. A detailed description of the method is available in previously published papers (e.g. [8, 12]). This measurement method was performed in accordance with the draft standard methods for high temperature corrosion assessments [4, 5].

Results and Discussion

Microstructural Investigations

Figure 2 shows back-scattered electron images of the cross-sections of T92, 347 HFG and HR3C following 1,000 h of exposure at 600, 650, and 700 °C in simulated air-fired combustion gases (1,300 vppm SO_2, 400 vppm HCl) without any deposit (D0). A thick multilayered oxide scale formed on T92 alloy, with voids within the scale, at all three temperatures. The scale formed at the lowest temperature (600 °C) is more compact than those from the other two temperatures. Measurements on these cross-sections show that the scale thickness on T92 increased from 600 to 650 °C. The oxide scale at 650 °C shows buckling of the outer layer (due to stresses in the scale), which had resulted in its delamination from the inner oxide layers that remain attached to the substrate. At 700 °C, the scale on T92 had completely delaminated from the substrate, but the overall thickness of the scale had reduced. There was no sign of internal oxidation of T92 in the range of temperatures investigated in this study. As expected, the scales formed on austenitic alloys (347 HFG and HR3C) are much thinner than those formed on the lower Cr content ferritic alloy (T92). On 347HFG, the scales formed at 650 °C were thicker than those formed at either 600 or 700 °C; a similar trend was also observed in HR3C. Internal damage was observed in both the austenitic alloys, particularly at 650 °C. Generally, the results show that much thicker scales were formed on T92, with

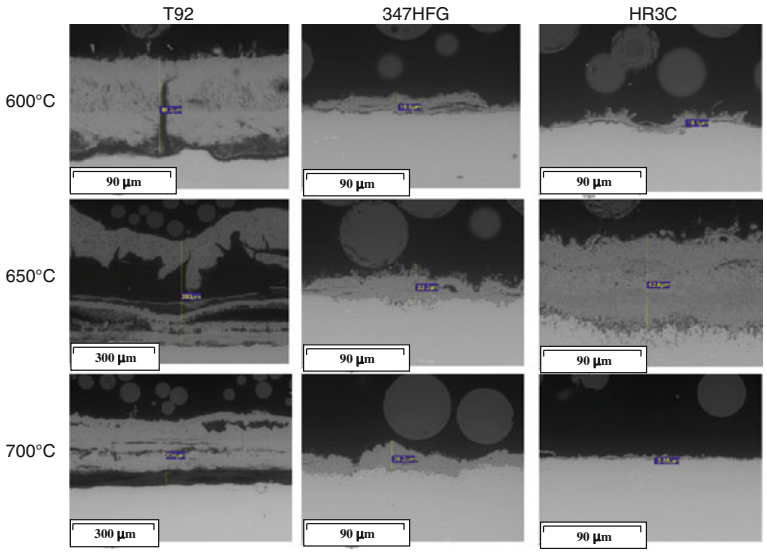

Fig. 2 BSE images of cross-sectioned scales on bare T92, 347HFG and HR3C exposed to simulated air-fired combustion gases (with 1,300 vppm SO_2/400 vppm HCl) at 600, 650 and 700 °C for 1,000 h

progressively thinner scales being formed on 347 HFG and HR3C (with increasing chromium content). These results are in line with the expected trend in scale development for these alloys [13, 14].

Figure 3 shows the BSE images of cross-sections through T92, 347HFG, HR3C and alloy 625 samples that had been covered in deposit D1 for 1,000 h at 600, 650, and 700 °C in simulated air-fired combustion gases (1,300 vppm SO_2, 400 vppm HCl). Deposit D1 is an aggressive deposit which can form alkali-iron tri-sulfate in combination with the simulated combustion environment. Alkali-iron tri-sulfate has frequently been identified as the key component for superheater/reheater corrosion in pulverized coal-fired boilers (i.e. when the gaseous environment combined with the exposure temperature generates sufficient SO_3 to stabilize this compound).

The microstructures of T92 at both 600 and 650 °C show that the scale/deposit layers are made up of compact inner layers and porous outer layers, but at 700 °C show a thicker band-like multi-layered structure. In all these cases the scale/deposit layers are significantly thicker than those formed without any deposit (i.e., compared with Fig. 2). The scale/deposit layers formed on the austenitic alloys (347 HFG and HR3C) are also very thick with numerous voids and examples of inter-layer delamination. At 600 °C HR3C showed the formation of relatively thin scale with good adhesion to the substrate; however, the scale/deposit layers were significantly thicker at 650 and 700 °C. At 600 °C the nickel-based alloy 625 showed scale/deposit layers, which were not apparent after exposure at 650 and 700 °C, possibly due to spallation. There was no clear evidence of internal damage in alloy 625 after the exposures in this study.

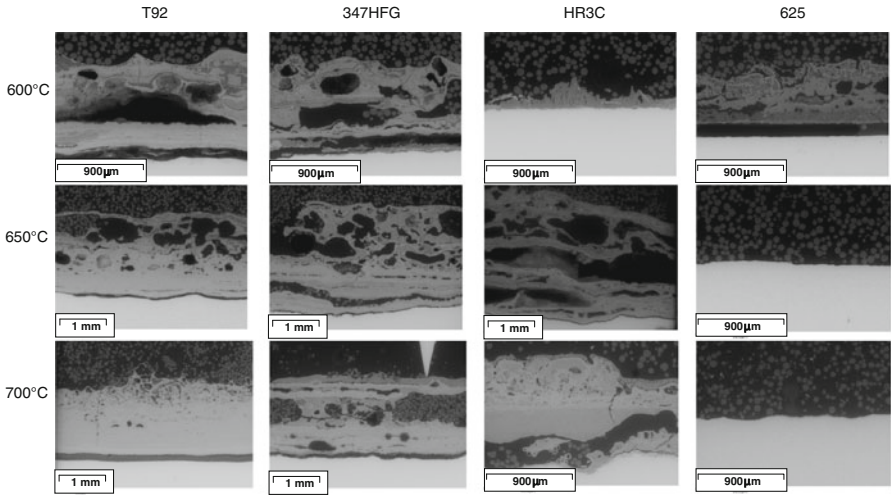

Fig. 3 BSE images of cross-sectioned scales on T92, 347HFG, HR3C and alloy 625 covered with deposit D1 exposed to simulated air-fired combustion gases at 600, 650 and 700 °C for 1,000 h

EDX mapping was carried out on many sample cross-sections. As an example, EDX maps of the ferritic alloy T92 (without any deposit and with deposit D1) exposed to simulated air-fired conditions at 650 °C for 1,000 h are shown in Fig. 4. The maps of the scale without any deposit (Fig. 4a) shows that oxygen and iron are distributed throughout the scale and chromium is enriched only in the inner layer of the scale, suggesting the inner scale is composed of a spinel layer (Fe, Cr-oxide, M_3O_4) and the outer layer is a thick layer of magnetite (Fe_3O_4) with a thin haematite (Fe_2O_3) layer at the scale/gas interface. Sulfur was detected at the scale/gas boundary and within the scale indicating a mixed oxidation/sulphidation attack. For the cross-section of T92 covered in deposit D1 (Fig. 4b), the EDX maps show that the molten deposits had infiltrated the scale during exposure as sulfur was found deep within the scale. Oxygen and iron are present throughout the scale/deposit and chromium is found only in the inner (spinel) oxide layer. Both sodium and potassium (from the applied deposit) were found in increasing concentrations towards the scale/gas interface, with the deposit/outer scale layer merging. The role of sulfur in the corrosion mechanism can be confirmed by the detection of a sulfur-rich layer at the inner scale.

Measurements of Metal Damage (Dimensional Metrology)

"Dimensional metrology" [4–7, 15] provides the best measurement of the corrosion performance of the different alloys, as it produces a distribution of metal damage data for each exposed sample. With regards to the draft standards for high temperature corrosion measurements [4, 5], the results are plotted as "change in metal thickness" (i.e. metal damage) as a function of cumulative probability. Figure 5 gives an example of "change in metal thickness" versus cumulative

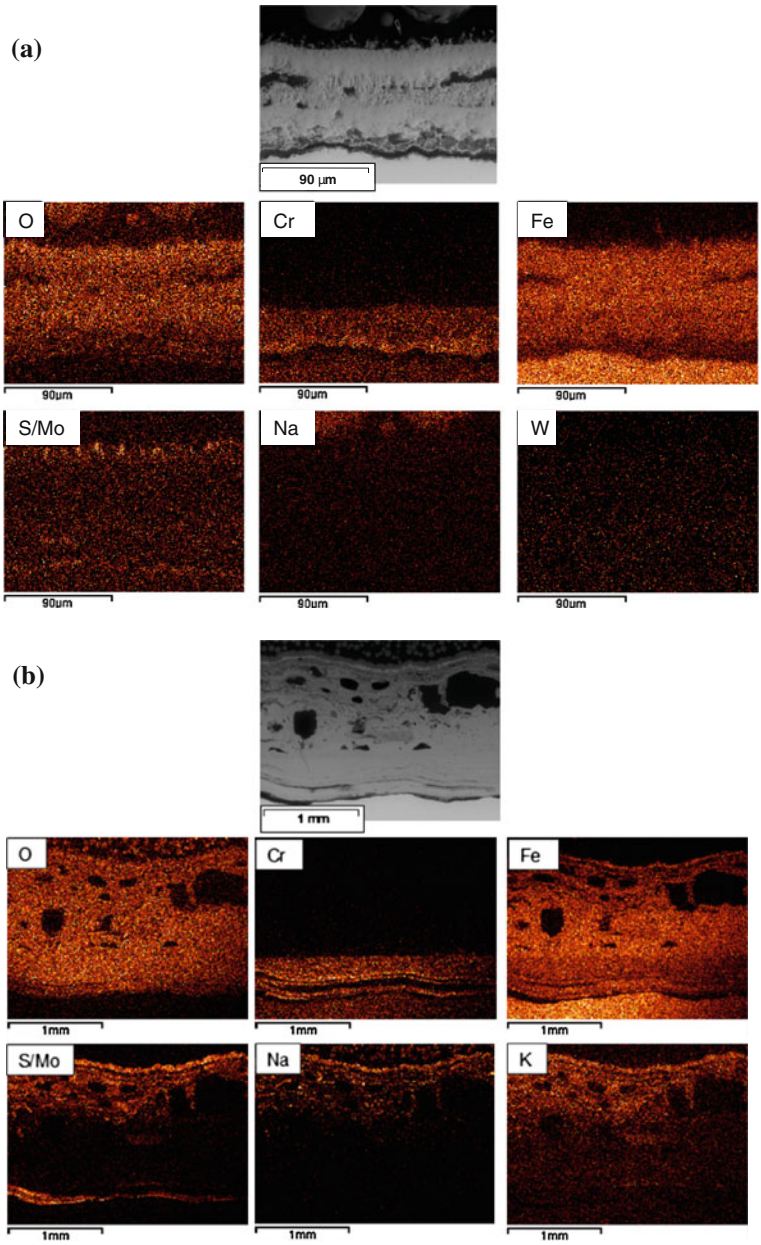

Fig. 4 BSE image and X-ray maps of cross-section through **a** bare T92 alloy **b** covered in deposit D1 exposed to simulated air-fired combustion gases (with 1,300 vppm SO_2/400 vppm HCl) at 650 °C for 1,000 h

probability for bare T92 exposed to simulated air-fired combustion gases at 600, 650 and 700 °C for 1,000 h (note that a larger "change in metal thickness" is more negative). These data show that the "change in metal thickness" at 600 °C was the

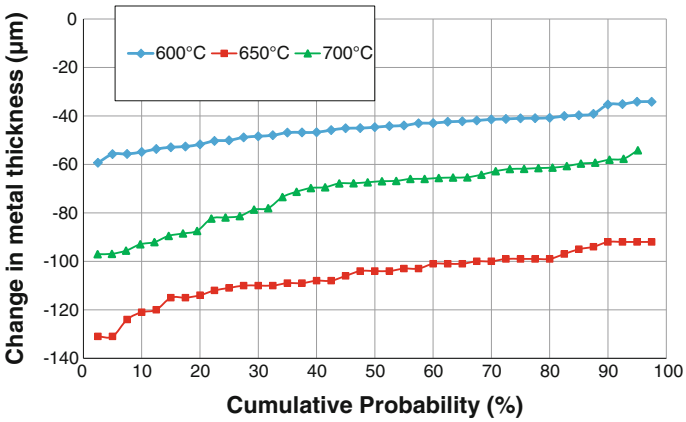

Fig. 5 Change in metal thickness versus cumulative probability for bare alloy T92 exposed to simulated air-fired combustion gases (with 1,300 vppm SO_2/400 vppm HCl) at different temperatures for 1,000 h

lowest of these three datasets, and that by increasing the test temperature to 650 °C the "change in metal thickness" had increased by more than a factor of two (looking at 50 % cumulative probability value of change in metal thickness). However, at the highest test temperature of 700 °C the "change in metal thickness" had decreased from its 650 °C value by ~30 %. This trend in metal loss data is in agreement with the ESEM scale thickness measurements and the mass change measurements [16].

The median "change in metal thickness" values, with the maximum and minimum values as error bars, for all alloys exposed in simulate air-fired condition without deposit (D0) and with deposit (D1) are shown in Fig. 6a, b, respectively. For the purpose of this paper, the "change in metal thickness" has been multiplied by "−1" and is presented as metal loss in Fig. 6. Figure 6a shows that the maximum metal loss for T92 without any applied deposit occurred at 650 °C. As shown by the distributions in Fig. 5, the metal loss on T92 increased by more than twice when the temperature was increased from 600 to 650 °C and subsequently

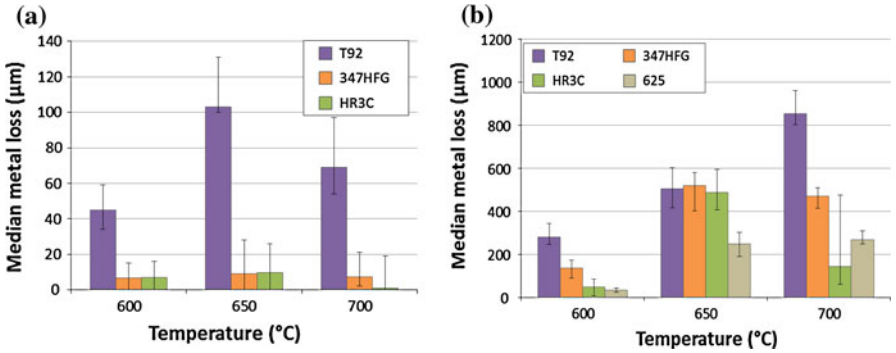

Fig. 6 Effect of temperature on median metal loss damage for **a** bare alloys and **b** alloys covered with deposit D1 after 1,000 h exposure in the simulated air-fired combustion gases

decreased by ~30 % when the temperature was further increased to 700 °C. Both austenitic alloys (347HFG and HR3C) also showed an increase in metal loss at 650 °C (looking at the maximum and minimum data ranges) but to a lesser extent compared to T92. Ferritic alloy (T92) resulted in a significantly higher damage (~4–10 times more) compared to the two austenitic alloys (347 HFG and HR3C) at all three temperatures. However, the increased chromium content of HR3C (25 wt% Cr) compared to 347HFG (18 wt% Cr), did not result in obvious reduction in metal loss at the lower temperatures.

It has been reported that at lower temperatures in mixed corrosive gases steels suffer from a combined oxidation and sulphidation attack which moves towards oxidation alone at the higher temperature [10]. For the reaction between SO_2 and O_2 to form SO_3, at lower temperatures SO_3 formation is favored but at higher temperatures SO_2 formation is favored [2, 11, 16]. The presence of SO_3 helps promote the mixed oxidation/sulphidation mechanism. In terms of damage levels, the rates for both mechanisms increase with temperature, but the mixed oxidation/sulphidation mechanism will be faster; thus the net effect will be to have a peak in damage levels when crossing the mechanism boundary with increasing temperature.

Figure 6b shows the median metal loss for the alloys covered in deposit D1 following exposure in simulated air-fired combustion gases for 1,000 h. Both ferritic (T92) and austenitic steels (347HFG & HR3C) showed considerably more damage when covered with deposit D1 than just exposed to the gaseous environment. All four alloys tested showed high levels of corrosion damage at 650 and 700 °C, especially when compared to generally acceptable superheater corrosion damage levels of 40–50 μm/1,000 h, but it should be noted that D1 is an aggressive deposit that is used to accelerate superheater corrosion damage in laboratory exposures. However, at 600 °C both HR3C and 625 still showed median metal losses of <50 μm even with this deposit. The median metal damage for steels at 600 and 700 °C had the following ranking (most to least damage): T92 > 347HFG > HR3C, which shows a strong dependence on the levels of Cr present in the alloys. However, at 650 °C, the metal losses for all three steels were very similar suggesting that even the 25 wt% Cr in HR3C could not develop a more protective scale than the 9 wt% Cr in T92 under this combination of exposure conditions. The nickel-based alloy 625 showed the best corrosion performance out of all four alloys at 600 and 650 °C, but was out-performed by HR3C at 700 °C.

The effect of temperature with deposit D1 on the austenitic steels (347HFG and HR3C) shows that the highest metal losses for both alloys were at 650 °C. This represents the characteristic "bell-shaped" curve for fireside corrosion damage that has been reported by several researchers [2, 17]. The peak in the corrosion rate is due to formation and then destabilization of molten complex alkali-iron tri-sulfates with increasing temperature. Alkali-iron-tri-sulfates melt at a much lower temperature than alkali sulfates, with a minimum melting point of ~550 °C compared to 832 °C [11, 16, 18–20]. However, alkali-iron tri-sulfates need to be stabilized by SO_3. The alkali-iron tri-sulfates formed from deposit D1 and the gas stream will have been molten at the exposure temperatures investigated here but will have solidified on cooling. The rate of corrosion increases with temperature in the presence of the molten deposits, but will then decrease when the complex sulfates

become unstable (due to the shift in the balance of SO_2/SO_3 towards SO_2 at higher temperature). The fireside corrosion rate has been reported to be at its highest between 650–680 °C by several investigators for air-fired conditions [2, 11, 16, 17], which is consistent with the results generated here. However, the "bell-shaped" curve was not seen in the ferritic alloy T92 which could be due to its inability to form more protective chromia scales, instead forming less protective iron-based oxide scales.

Conclusions

The effect of temperature (600, 650 and 700 °C) on the fireside corrosion of four different alloys (T92, 347 HFG, HR3C and 625) has been investigated with and without a synthetic deposit in simulated air-fired combustion conditions in a controlled atmosphere furnace for 1,000 h. The 'deposit recoat' exposures were targeted at a gaseous environment anticipated around superheaters/reheaters when air-firing a pulverized fuel mix of 20 wt% CCP with 80 % of a typical UK coal. "Dimensional metrology" of each of the samples was carried out to quantify the material damage due to fireside corrosion and generate metal loss distributions under specific exposure conditions. The microstructures of scales/deposits formed on the samples were studied on cross-sections using ESEM with EDX mapping.

It can be concluded that under all the exposure conditions the ferritic alloy (T92) proved to be the poorest performing alloy. At all exposure temperatures the combination of the gaseous environment and deposit D1 (generating alkali-iron tri-sulfate compounds) was found to damage all the alloys significantly more than just gaseous environment alone. The trend in metal damage on alloys exposed without deposit showed a reduction at higher temperature due to a shift in corrosion mechanisms from mixed oxidation/sulphidation to oxidation only; this was especially marked for T92. The trend in metal damage of the austenitic steels (347HFG & HR3C) when exposed with deposit D1 showed a "bell-shaped" curve, which is characteristic of superheater fireside corrosion damage, with the highest damage levels observed at 650 °C (and a peak in the damage anticipated to be in the range 650–700 °C). This reduction of metal damage at higher temperature in deposit induced fireside corrosion is believed to be due to changes in the stability of the complex alkali-iron-tri-sulfates, which need SO_3 to stabilize them and so are favored at the lower temperatures used.

Acknowledgments The authors acknowledge the support of The Energy Programme, which is a Research Councils UK cross council initiative led by EPSRC and contributed to by ESRC, NERC, BBSRC and STFC, and specifically the Supergen initiative (Grants GR/S86334/01 and EP/F029748) and the following companies; Alstom Power Ltd., Doosan Babcock, E.ON, National Physical Laboratory, Praxair Surface Technologies Ltd, QinetiQ, Rolls-Royce plc, RWE npower, Siemens Industrial Turbomachinery Ltd. and Tata Steel, for their valuable contributions to the project.

References

1. A. A. Khan, W. de Jong, P. J. Jansens and H. Spliethoff, *Fuel Processing Technology* **90**, 21 (2009).
2. J. Stringer and I. G. Wright, *Oxidation of Metals* **44**, 265 (1995).

3. N. J. Simms, P. J. Kilgallon, and J. E. Oakey, *Energy Materials: Material Science and Engineering for Energy System*, **2** (2007).
4. *Draft Code of Practice for Discontinuous Corrosion Testing in High Temperature Gaseous Atmospheres.* EC project SMT4-CT95-2001, TESTCORR. (ERA Technology, Surrey, 2000).
5. *Corrosion of Metals and Alloy—Method for Metallographic Examination of Samples After Exposure to High Temperature Corrosive Environments*. Draft ISO standard. ISO/TC 156 NWI 5092005 (2006).
6. S. R. J. Saunders, in *Guidelines for Methods of Testing and Research in High Temperature Corrosion*, eds. H. J. Grabke and D. B. Meadowcroft (The Institute of Metals, London, 1995), p. 85.
7. N. J. Simms and A. T. Fry, in *Materials for Advanced Power Engineering, Proceedings*, eds. J. Lecomte-Beckers and M. Carton (Forschungszentrum Jülich GmbH, 2010).
8. A. U. Syed, N. J. Simms, and J. E. Oakey, "Fireside corrosion of superheaters: effects of air and oxy-firing of coal and biomass", *Fuel* (in press).
9. E. Raask, *Mineral Impurities in Coal Combustion*, (Hemisphere Publishing Corporation, Washington DC, 1985).
10. K. Natesan, A. Purohit, and D. L. Rink. *US Department of Energy Fossil Energy Conference* (2003).
11. N. J. Simms, in *Power Plant Life Management and Performance Improvement*, ed. J. E. Oakey (Woodhead Publishing, Cambridge, 2011), p. 145.
12. J. R. Nicholls, N. J. Simms, and A. Encinas-Oropesa, *Mats at High Temperatures* **24**, 149 (2007).
13. D. Young, *High Temperature Oxidation and Corrosion of Metals*, (Elsevier, Amsterdam, 2008).
14. N. Birks, G. H. Meier, and F. S. Pettit, *High-Temperature Oxidation of Metals*, (Cambridge University, Cambridge, 2006).
15. J. R. Nicholls and P. Hancock, *NACE-6*, ed. R. A. Rapp, (1983), p. 198.
16. A. U. Syed, "*Fireside Corrosion Study of Superheater Materials in Advanced Power Plants*", PhD thesis.
17. W. T. Reid, *External Corrosion and deposits: Boilers and Gas Turbines*, (Elsevier, New York, 1971).
18. A. Hendry, *Corrosion Science* **20**, 383 (1980).
19. C. Cain and W. Nelson, *Transactions of the ASME, Journal of Engineering Power* **83**, 468 (1961).
20. D. Lindberg, R. Backman, and P. Chartrand, *Journal of Chemical Thermodynamics* **39**, 1001 (2007).